Article:
Zhu, Y.-P., Lang, Z.Q., Mao, H.-L. et al. (2022) Nonlinear output frequency response functions: A new evaluation approach and applications to railway and manufacturing systems' condition monitoring. Mechanical Systems and Signal Processing, 163. 108179. ISSN: 0888-3270

https://doi.org/10.1016/j.ymssp.2021.108179

Nonlinear Output Frequency Response Functions: A New Evaluation Approach and Applications to Railway and Manufacturing Systems' Condition Monitoring

Yun-Peng Zhu[1], Z Q Lang[1]*, Han-Ling Mao[2], Hatim Laalej[3]

1. Department of Automatic Control and Systems Engineering, The University of Sheffield, Sheffield, S1 3JD, U.K.

2. School of Mechanical Engineering, Guangxi University, Nanning, 530004, China.

3. Advanced Manufacturing Research Centre, University of Sheffield, Sheffield, U.K.

*e-mail: z.lang@sheffield.ac.uk

Abstract: The Nonlinear Output Frequency Response Functions (NOFRFs) are an extension of the well-known Frequency Response Function (FRF) of linear systems to the nonlinear case and have recently been applied by many researchers to resolve different engineering problems. However, there exist several issues with current methods that can be used for the evaluation of the NOFRFs of practical systems. These include the difficulty and lack of an effective approach of accurately evaluating the NOFRFs for a general class of nonlinear systems. In the present study, a new concept known as the Generalized Associated Linear Equations (GALEs) is introduced to develop a novel approach to systematically address these problems. By using the GALEs, the NOFRFs of the NARX (Nonlinear Auto Regressive with eXegenous input) model or NDE (Nonlinear Differential Equation) model of nonlinear systems can be accurately evaluated by simply dealing with the solutions to a series of linear difference or differential equations. This can significantly facilitate the NOFRFs based nonlinear system analyses and associated practical applications. Two experimental studies including monitoring fatigue damage of train wheels and inspecting wearing conditions of cutting tools, respectively, demonstrate the significance and potential applications of the new GALEs based NOFRFs evaluation in railway and manufacturing systems' condition monitoring.

Key words: Condition monitoring; Nonlinear systems; Generalized Associated Linear Equations (GALEs); Frequency domain; Nonlinear Output Frequency Response Functions (NOFRFs).

1. Introduction

It is well known that the Frequency Response Function (FRF) is a fundamental concept of linear systems, is the theoretical basis of classical control and structural system design and analysis, and has been widely applied in engineering practice [1,2]. The traditional extension of the FRF concept to the nonlinear case is known as the Generalized Frequency Response Functions (GFRFs), which were derived based on the Volterra series theory of nonlinear systems [3]. The GFRFs are a series of multi-dimensional complex functions of frequencies representing the frequency domain characteristics of nonlinear systems with different orders of nonlinearity. Since proposed in late 1950s, the GFRFs have been exploited to analytically study weakly nonlinear systems [4] and to qualitatively evaluate the nonlinear characteristics of some mechanical, sensor, and bioengineering systems [5-7]. However, due to the multi-dimensional nature of the GFRFs, it is still rare to see the application of the GFRFs to literally resolve more

complicated engineering problems.

In order to address this problem, in the last decades, several one-dimensional frequency domain representations of nonlinear systems have been proposed. These include, for example, the Nonlinear Output Frequency Response Functions (NOFRFs) [8], the Output Frequency Response Function (OFRF) [9] and the Higher Order Sinusoidal Input Describing Functions (HOSIDF) [10]. The OFRF can be used to facilitate the design of nonlinear systems in the frequency domain [11,12]; The HOSIDF is dedicated to the study of nonlinear systems subject to sinusoidal inputs [13]; while the NOFRFs are a series of one-dimensional functions of frequency variable, providing a series of Bode plot like frequency domain representations and a novel framework for the analysis of nonlinear systems in the frequency domain [14].

The NOFRFs based nonlinear system analysis basically involves the evaluation of the NOFRFs of a nonlinear system under study and the use of the evaluated NOFRFs or associated indices to reveal the system's dynamic properties [15,16]. This has, very recently, found a wide range of applications especially in the condition monitoring and fault diagnosis of engineering structural systems [15-19].

The fundamental idea of the application of the NOFRFs to the engineering structural systems' condition monitoring and fault diagnosis is as illustrated in Fig.1, involving:

(i) Using the system input/output data to either directly evaluate the NOFRFs [15] or to identify an input/output model and then evaluate the NOFRFs using the identified model [14,18].

(ii) Extracting the dynamic features of the underlying system from the evaluated NOFRFs and carrying out the system's condition monitoring and fault diagnosis using an index based on the extracted features [18].

The advantage of this condition monitoring and fault diagnosis scheme over widely used signal analyses are that the NOFRFs features and associated index can more directly reveal inherent dynamics of inspected systems which are often much more relevant to systems' operational or faulty conditions than signal features [14,20]. In addition, it is worth noting that the paradigm shown in Fig.1 with NOFRFs replaced by FRF has already been widely used in engineering practice for the identification of the dynamic properties of linear engineering structures, systems or components. Typical examples include, for example, modal analysis of buildings and bridges [21] and study of electrical impedance spectroscopy of functional materials [22]. However, as far as we are aware of, the NOFRFs approach has, for the first time, enabled this paradigm to be applicable to nonlinear engineering structures and systems in a systematical way.

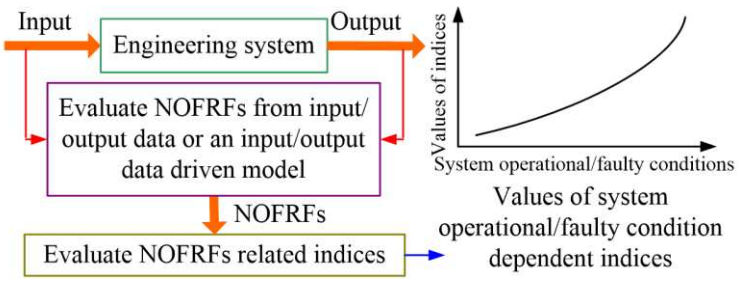

Fig.1 The NOFRFs based engineering system condition monitoring/fault diagnosis

One of the key issues with the realization of the paradigm shown in Fig.1 in practice is how to effectively evaluate the NOFRFs for a nonlinear system under study. Currently, most researchers use a Least Squares (LS) based algorithm

[8] to determine the NOFRFs directly from the system input/output data [15]. This algorithm requires conducting specific experiments on inspected structures or systems and cannot accurately determine the NOFRFs up to any order of system nonlinearity of interest due to the truncation error associated with the Volterra series representation of a nonlinear system. In order to address this problem, recently, a method was proposed in [14] based on the Associated Linear Equation (ALE) [23,24]. This technique can be applied to an NARX (Nonlinear Auto Regressive with eXegenous input) model of nonlinear system under study identified from the system input/output data to accurately compute the system NOFRFs up to any order of nonlinearity. However, this method involves a relatively complicated procedure including solving Diophantine equations that are not straightforward to use in practice especially for nonlinear systems that have to be represented by a more complicated NARX model.

In order to resolve the problems with existing approaches for the NOFRFs evaluation, in the present study, the concept of the Generalized Associated Linear Equations (GALEs) is proposed, extending the ALEs to a wide class of nonlinear systems that can be described by a polynomial difference/differential equation model, known as the NARX or NDE (Nonlinear Differential Equation) model of nonlinear systems. An effective algorithm is then derived, which can readily be used to determine the GALEs directly from the system's NARX or NDE model using a simple recursive procedure circumventing the difficulties with solving Diophantine equations associated with the technique in [14]. In the cases where an appropriate NARX or NDE model of the nonlinear system of concern can be identified, the GALEs thus determined allow an accurate evaluation of the NOFRFs up to any order of system nonlinearity simply from the solutions to a series of linear difference or differential equations.

In conjunction with a nonlinear system identification method such as, for example, the NARMAX method [25], the new NOFRFs evaluation approach can be used in various practical applications including engineering system condition monitoring and fault diagnosis. To show this, two experimental studies are carried out to monitor fatigue damage of train wheels and inspect wearing conditions of cutting tools, respectively. The results demonstrate the significance and potential applications of the novel GALEs based NOFRFs evaluation in railway and manufacturing systems' condition monitoring.

2. Generalized Associate Linear Equations (GALEs) of the NARX and NDE models of nonlinear systems

2.1 The GFRFs of nonlinear systems

In practice, a large class of nonlinear systems can be described by a discrete-time NARX model [26]

$$y(k)=\sum_{m=1}^{M}\sum_{p=0}^{m}\sum_{k_1,\,k_{p+q}=1}^{K}\left[c_{p,q}\left(k_1,\cdots,k_{p+q}\right)\prod_{i=1}^{p}y\left(k-k_i\right)\prod_{i=p+1}^{p+q}u\left(k-k_i\right)\right] \tag{1}$$

where k represents the discrete time, M and K are integers, and $p+q=m$; $\sum_{k_1,\,k_{p+q}=1}^{K}=\sum_{k_1=1}^{K}\cdots\sum_{k_{p+q}=1}^{K}$ and $c_{p,q}\left(k_1,\cdots,k_{p+q}\right)$ are the coefficients of model (1).

If system (1) is asymptotically stable at the zero equilibrium, the output can be represented by a discrete Volterra series as [3]:

$$y(k)\approx\sum_{n=1}^{N}y_n(k)=\sum_{n=1}^{N}\sum_{\tau_1=-\infty}^{+\infty}\cdots\sum_{\tau_n=-\infty}^{+\infty}h_n(\tau_1,\ldots,\tau_n)\prod_{i=1}^{n}u(k-\tau_i) \tag{2}$$

where N is the maximum order of the system's nonlinearity, $y_n(k), n=1,...,N$, is the output component of system (1) contributed by the system's nth order nonlinearity and known as the nth order nonlinear output of the system, and $h_n(\tau_1,\ldots,\tau_n)$ is called the nth order Volterra kernel of the system. In the frequency domain, the output spectrum $Y(\mathrm{j}\omega)$ of system (2) can be represented as [27]

$$Y(\mathrm{j}\omega)\approx\sum_{n=1}^{N}Y_n(\mathrm{j}\omega)=\sum_{n=1}^{N}\frac{1}{\sqrt{n}(2\pi)^{n-1}}\int_{\omega_1+\cdots+\omega_n=\omega}H_n(\omega_1,\ldots,\omega_n)\prod_{i=1}^{n}U(\mathrm{j}\omega_i)\mathrm{d}\sigma_\omega \tag{3}$$

In (3), $Y_n(\mathrm{j}\omega)$ is the spectrum of $y_n(k)$ obtained by the normalised Discrete Time Fourier Transform (nDTFT) under the sampling time of Δt [28]. $\int_{\omega_1+\cdots+\omega_n=\omega}[.]\mathrm{d}\sigma_\omega$ denotes the integration carried out over the hyperplane $\omega_1+\cdots+\omega_n=\omega$ with $\mathrm{d}\sigma_\omega$ representing an infinitely small element on the hyperplane, $U(\mathrm{j}\omega_i)$ represents the input spectrum at the frequency ω_i, and

$$H_n(\omega_1,\ldots,\omega_n)=\Delta t\sum_{\tau_1=-\infty}^{+\infty}\cdots\sum_{\tau_n=-\infty}^{+\infty}h_n(\tau_1,\ldots,\tau_n)\exp\left(-\mathrm{j}\left(\omega_1\tau_1\Delta t+\cdots+\omega_n\tau_n\Delta t\right)\right)$$

is the nth order GFRF of the system, which can be determined from the NARX model (1) using a recursive algorithm as follows [26]

$$\begin{aligned}&\left\{1-\sum_{k_1=1}^{K}c_{1,0}(k_1)\exp\left[-\mathrm{j}\left(\omega_1+\cdots+\omega_n\right)k_1\Delta t\right]\right\}H_n(\omega_1,\cdots,\omega_n)\\&=\sum_{k_1,\,k_n=1}^{K}c_{0,n}(k_1,\cdots,k_n)\exp\left[-\mathrm{j}\left(k_1\omega_1+\cdots+k_n\omega_n\right)\Delta t\right]\\&+\sum_{q=1}^{n-1}\sum_{p=1}^{n-q}\sum_{k_1,\,k_{p+q}=1}^{K}\left\{c_{p,q}(k_1,\cdots,k_{p+q})H_{n-q,p}^{\mathbf{K}_{p+q}}(\omega_1,\cdots,\omega_{n-q})\exp\left[-\mathrm{j}\left(k_{p+1}\omega_{n-q+1}+\cdots+k_{p+q}\omega_n\right)\Delta t\right]\right\}\\&+\sum_{p=2}^{n}\sum_{k_1,\,k_p=1}^{K}\left[c_{p,0}(k_1,\cdots,k_p)H_{n,p}^{\mathbf{K}_p}(\omega_1,\cdots,\omega_n)\right]\end{aligned} \tag{4}$$

where

$$\begin{cases}H_{n,p}^{\mathbf{K}_p}(\omega_1,\cdots,\omega_n)=\sum_{i=1}^{n-(p-1)}H_i(\omega_1,\cdots,\omega_i)H_{n-i,p-1}^{\mathbf{K}_p}(\omega_{i+1},\cdots,\omega_n)\exp\left[-\mathrm{j}k_p\left(\omega_1+\cdots+\omega_i\right)\Delta t\right]\\H_{n,1}^{\mathbf{K}_1}(\omega_1,\cdots,\omega_n)=H_n(\omega_1,\cdots,\omega_n)\exp\left[-\mathrm{j}k_1\left(\omega_1+\cdots+\omega_n\right)\Delta t\right]\end{cases} \tag{5}$$

with $n=1,\ldots,N$, and $\mathbf{K}_n=(k_1,\ldots,k_n)$.

2.2 The NOFRFs of nonlinear systems

It can be observed that the GFRFs of nonlinear systems are multi-dimensional functions, which are difficult to be applied in practice. To address this issue, the NOFRFs of nonlinear systems are introduced as

$$G_n(\mathrm{j}\omega)=\frac{Y_n(\mathrm{j}\omega)}{U_n(\mathrm{j}\omega)};\ \omega\in\Omega \tag{6}$$

where $Y_n(\mathrm{j}\omega)$ and $U_n(\mathrm{j}\omega)$ are the nth order output spectrum and the nth order generalized input spectrum that can obtained by the nDTFT of $y_n(k)$ and $u^n(k)$, respectively; Ω is the frequency support of $|U_n(\mathrm{j}\omega)|$, which can be determined using the results about the output frequencies of nonlinear systems [27]. From equation (3) and (6), the output spectrum of nonlinear system (2) can be represented as

$$Y(\mathrm{j}\omega) \approx \sum_{n=1}^{N} Y_n(\mathrm{j}\omega) = \sum_{n=1}^{N} G_n(\mathrm{j}\omega) U_n(\mathrm{j}\omega) \tag{7}$$

It is obvious that, when $n = N = 1$, $G_n(\mathrm{j}\omega) = G_1(\mathrm{j}\omega)$ reduces to the FRF of a linear system. The NOFRFs are one-dimensional functions that enable the evaluation of the system frequency domain characteristics using a series of Bode plot like diagrams. This advantage of the NOFRFs has already been exploited to perform frequency analysis for condition monitoring, fault diagnosis, and modal analysis of practical nonlinear systems [14-16,19].

The NOFRFs can be evaluated by using a LS based algorithm [8], which requires the system output response to inputs with different amplitudes and an appropriate selection of the maximum order N of system nonlinearity. Although Bayma et al [14] has proposed a method based on the concept of Associated Linear Equations (ALE) to address the problem with the LS based algorithm, the ALE based method involves a relatively complicated procedure to solve Diophantine equations that are not straightforward to implement in practice especially for systems that have to be described by a more complicated NARX model.

In order to circumvent the difficulties with using exiting methods for the NOFRFs evaluation, a novel approach is proposed in the present study, which is based on a newly introduced concept known as the Generalized Associated Linear Equations (GALEs).

2.3 The GALEs of nonlinear systems

By multiplying each side of equation (4) with $\prod_{i=1}^{n} U(\mathrm{j}\omega_i)$ and evaluating the integration of the result over the hyperplane $\omega_1 + \cdots + \omega_n = \omega$, it can be shown that

$$Y_n(\mathrm{j}\omega) = \tilde{H}(\mathrm{j}\omega) V_n(\mathrm{j}\omega); n = 1, \ldots, N \tag{8}$$

where

$$\begin{cases} \tilde{H}(\mathrm{j}\omega) = \left[1 - \sum_{k_1=1}^{K} c_{1,0}(k_1) \exp(\mathrm{j}k_1\omega\Delta t) \right]^{-1} \\ V_n(\mathrm{j}\omega) = \dfrac{1}{\sqrt{n}(2\pi)^{n-1}} \int_{\omega_1 + \cdots + \omega_n = \omega} \left(\Psi_{n,u} + \Psi_{n,uy} + \Psi_{n,y} \right) \prod_{i=1}^{n} U(\mathrm{j}\omega_i) \mathrm{d}\sigma_\omega \end{cases} \tag{9}$$

with

$$\Psi_{n,u} = \sum_{k_1, k_n=1}^{K} c_{0,n}(k_1, \cdots, k_n) \exp\left[-\mathrm{j}(k_1\omega_1 + \cdots + k_n\omega_n)\Delta t \right] \tag{10}$$

$$\Psi_{n,uy}=\sum_{q=1}^{n-1}\sum_{p=1}^{n-q}\sum_{k_1,k_{p+q}=1}^{K}\left\{c_{p,q}\left(k_1,\cdots,k_{p+q}\right)H_{n-q,p}^{\mathbf{K}_{p+q}}\left(\omega_1,\cdots,\omega_{n-q}\right)\right.$$
$$\left.\times\exp\left[-\mathrm{j}\left(k_{p+1}\omega_{n-q+1}+\cdots+k_{p+q}\omega_n\right)\Delta t\right]\right\} \tag{11}$$

and

$$\Psi_{n,y}=\sum_{p=2}^{n}\sum_{k_1,k_p=1}^{K}\left[c_{p,0}\left(k_1,\cdots,k_p\right)H_{n,p}^{\mathbf{K}_p}\left(\omega_1,\cdots,\omega_n\right)\right] \tag{12}$$

It is obvious that (8) is the frequency domain representation of a linear system, where $\tilde{H}\left(\mathrm{j}\omega\right)$ is the frequency response function and $V_n\left(\mathrm{j}\omega\right)$ is the input spectrum of this linear system. By applying the inverse nDTFT to both sides of equation (8), this linear system can be described in the time domain as

$$f_{\mathrm{lin}}\left[y_n\left(k\right)\right]=v_n\left(k\right),\ n=1,\ldots,N \tag{13}$$

where $v_n\left(k\right)$ is the inverse nDTFT of $V_n\left(\mathrm{j}\omega\right)$ and $f_{\mathrm{lin}}\left[.\right]$ denotes a linear difference operator.

Equation (13) is referred to as the GALEs of nonlinear system (1). Obviously, given $f_{\mathrm{lin}}\left[.\right]$ and $v_n\left(k\right)$, from the GALEs (13), $y_n\left(k\right)$ can readily be found by solving a simple linear difference equation. Therefore, the determination of the GALEs can facilitate determining $y_n\left(k\right)$ so as to evaluate the NOFRFs for a very wide class of nonlinear systems, which are, as defined in (6), the ratio between the nDTFT of $y_n\left(k\right)$ and the nDTFT of $u^n\left(k\right)$ for $n=1,\ldots,N$.

2.4 Determination of the GALEs

The GALEs of the NARX model (1) of nonlinear systems can be determined by using Proposition 1 as follows.

Proposition 1. *The GALEs of the NARX model (1) of nonlinear systems can be determined as*

$$y_n\left(k\right)-\sum_{k_1=1}^{K}c_{1,0}\left(k_1\right)y_n\left(k-k_1\right)=\sum_{k_1,k_n=1}^{K}c_{0,n}\left(k_1,\cdots,k_n\right)\prod_{i=1}^{n}u\left(k-k_i\right)$$
$$+\sum_{q=1}^{n-1}\sum_{p=1}^{n-q}\sum_{k_1,k_{p+q}=1}^{K}c_{p,q}\left(k_1,\cdots,k_{p+q}\right)y_{n-q,p}^{\mathbf{K}_{p+q}}\left(k\right)\prod_{i=p+1}^{p+q}u\left(k-k_i\right) \tag{14}$$
$$+\sum_{p=2}^{n}\sum_{k_1,k_p=1}^{K}c_{p,0}\left(k_1,\cdots,k_p\right)y_{n,p}^{\mathbf{K}_p}\left(k\right)$$

where $n\geq 1$, $\mathbf{K}_n=\left(k_1,\ldots,k_n\right)$ *and*

$$y_{n,p}^{\mathbf{K}_p}\left(k\right)=\sum_{i=1}^{n-(p-1)}y_i\left(k-k_p\right)y_{n-i,p-1}^{\mathbf{K}_p}\left(k\right) \tag{15a}$$

and

$$y_{n,1}^{\mathbf{K}_1}\left(k\right)=y_n\left(k-k_1\right) \tag{15b}$$

Proof of Proposition 1. See Appendix A.

By comparing equations (4) and (14), it can be observed that the algorithms for the evaluation of the GFRFs and the GALEs, respectively, have a significant similarity. This implies $y_n\left(k\right)$, $y_{n-p,q}^{\mathbf{K}_{p+q}}\left(k\right)$ in Proposition 1 can theoretically be

interpreted as the time domain analogy of $H_n(\omega_1,\cdots,\omega_n)$, $H_{n-p,q}^{\mathbf{K}_{p+q}}(\omega_1,\cdots,\omega_{n-p})$ in equation (4), revealing a novel and interesting relationship between the time and frequency domain properties of nonlinear systems. In addition, by comparing equation (14) with equation (13), it is known that $f_{\text{lin}}[.]$ and $v_n(k)$ in the GALEs (13) can be determined directly from the NARX model (1) of nonlinear systems as follows

$$f_{\text{lin}}\left[y_n(k)\right]=y_n(k)-\sum_{k_1=1}^{K}c_{1,0}(k_1)\,y_n(k-k_1)$$

$$\begin{aligned}v_n(k)=&\sum_{k_1,k_n=1}^{K}c_{0,n}(k_1,\cdots,k_n)\prod_{i=1}^{n}u(k-k_i)\\&+\sum_{q=1}^{n-1}\sum_{p=1}^{n-q}\sum_{k_1,\,k_{p+q}=1}^{K}c_{p,q}(k_1,\cdots,k_{p+q})\,y_{n-q,p}^{\mathbf{K}_{p+q}}(k)\\&\times\prod_{i=p+1}^{p+q}u(k-k_i)+\sum_{p=2}^{n}\sum_{k_1,\,k_p=1}^{K}c_{p,0}(k_1,\cdots,k_p)\,y_{n,p}^{\mathbf{K}_p}(k)\end{aligned}$$

Taking into account equation (15), the above expression of $v_n(k)$ shows that $v_n(k)$ is dependent on the system input in the past $u(k-1),\ldots,u(k-K)$ as well as the system output components contributed by the system nonlinearities up to the $(n-1)$th order $y_{n-1}(k),\cdots,y_1(k)$. Therefore, the GALEs determined using Proposition 1 provide a powerful recursive algorithm that can readily be used to find the output components of nonlinear system (1) contributed by system nonlinearity up to any order of concern.

For example, for the unplugged Van der Pol system [29]

$$m\ddot{y}(t)+c\dot{y}(t)+ky(t)+c_E y^2(t)\,\dot{y}(t)=u(t) \tag{16}$$

where m,c,k and c_E are system linear and nonlinear parameters, respectively, the NARX model can be obtained by discretizing the model (16) to yield [12]:

$$\begin{aligned}y(k)=&\,c_{0,1}(1)u(k-1)+c_{1,0}(1)\,y(k-1)+c_{1,0}(2)\,y(k-2)\\&+c_{3,0}(1,1,1)\,y^3(k-1)+c_{3,0}(1,1,2)\,y^2(k-1)\,y(k-2)\end{aligned} \tag{17}$$

with

$$\begin{aligned}&c_{0,1}(1)=\frac{\Delta t^2}{m};\ c_{1,0}(1)=2-\frac{\Delta tc}{m}-\frac{\Delta t^2k}{m};\ c_{1,0}(2)=\frac{\Delta tc}{m}-1;\\&c_{3,0}(1,1,1)=-\frac{\Delta tc_E}{m};\ c_{3,0}(1,1,2)=\frac{\Delta tc_E}{m}\end{aligned} \tag{18}$$

The GALEs of the NARX model (17) can be determined using Proposition 1 as follows

For $n=1$

$$y_1(k)=c_{0,1}(1)u(k-1)+c_{1,0}(1)\,y_1(k-1)+c_{1,0}(2)\,y_1(k-2) \tag{19}$$

For $n=2$

$$y_2(k)=c_{1,0}(1)\,y_2(k-1)+c_{1,0}(2)\,y_2(k-2)=0 \tag{20}$$

For $n=3$

$$y_3(k)=c_{1,0}(1)y_3(k-1)+c_{1,0}(2)y_3(k-2)+c_{3,0}(1,1,1)y_{3,3}^{(1,1,1)}(k)+c_{3,0}(1,1,2)y_{3,3}^{(1,1,2)}(k) \tag{21}$$

where

$$y_{3,3}^{(1,1,1)}(k)=y_1(k-1)y_{2,2}^{(1,1,1)}(k)=y_1^{\,2}(k-1)y_{1,1}^{(1,1,1)}(k)=y_1^{\,3}(k-1) \tag{22a}$$

$$y_{3,3}^{(1,1,2)}(k)=y_1(k-2)y_{2,2}^{(1,1,2)}(k)=y_1(k-2)y_1(k-1)y_{1,1}^{(1,1,2)}(k)=y_1(k-2)y_1^{\,2}(k-1) \tag{22b}$$

Clearly, proceeding with this process, one can produce the GALEs associated with a system NARX model up to any order n of system nonlinearity of interest.

The above results about the GALEs of the NARX model can readily be extended to the NDE model of nonlinear systems [30]:

$$\sum_{m=1}^{M}\sum_{p=0}^{m}\sum_{l_1,\,l_{p+q}=0}^{L}\left[c_{p,q}(l_1,\cdots,l_{p+q})\prod_{i=1}^{p}D^{l_i}y(t)\prod_{i=p+1}^{p+q}D^{l_i}u(t)\right]=0 \tag{23}$$

where M and L are integers; $p+q=m$; D is the differential operator defined by $D^l x(t)=\mathrm{d}^l x(t)/\mathrm{d}t^l$; $c_{p,q}(l_1,\cdots,l_{p+q})$ are the coefficients of model (23).

The GALEs of the NDE model (23) is a series of linear differential equations with regard to $y_n(t), n=1,\ldots,N$, the output component contributed by the n th order nonlinearity of the system. The GALEs of the NDE model (23) can be obtained by using Proposition 2 as follows.

Proposition 2. *The GALEs of the NDE model (23) of nonlinear systems can be obtained as*

$$\begin{aligned}-\sum_{l_1=0}^{L}c_{1,0}(l_1)D^{l_1}y_n(t)&=\sum_{l_1,l_n=0}^{L}c_{0,n}(l_1,\cdots,l_n)\prod_{i=1}^{n}D^{l_i}u(t)\\&+\sum_{q=1}^{n-1}\sum_{p=1}^{n-q}\sum_{l_1,\,l_{p+q}=0}^{L}c_{p,q}(l_1,\cdots,l_{p+q})y_{n-q,p}^{\mathbf{L}_{p+q}}(t)\prod_{i=p+1}^{p+q}D^{l_i}u(t)\\&+\sum_{p=2}^{n}\sum_{l_1,\,l_p=0}^{L}c_{p,0}(l_1,\cdots,l_p)y_{n,p}^{\mathbf{L}_p}(t)\end{aligned} \tag{24}$$

where $n\geq 1$, $\mathbf{L}_n=(l_1,\ldots,l_n)$ *and*

$$y_{n,p}^{\mathbf{L}_p}(t)=\sum_{i=1}^{n-(p-1)}D^{l_p}y_i(t)\,y_{n-i,p-1}^{\mathbf{L}_p}(t) \tag{25a}$$

and

$$y_{n,1}^{\mathbf{L}_1}(t)=D^{l_1}y_n(t) \tag{25b}$$

Proof of Proposition 2. Proposition 2 can be proven in a way similar to the proof for Proposition 1.

It is worth mentioning that the ALEs in [23,24] are a special case of the GALEs and were proposed for relatively simple Duffing type continuous time nonlinear systems. For example, the ALEs can't be directly applied to Van der Pol system (16) in which there is an additional damping term $y^2(t)\dot{y}(t)$. The GALEs are an extension of the ALEs and can be used to analyse a very general class of nonlinear systems that can be represented by a NARX or NDE model.

3. The GALEs based evaluation of the NOFRFs of nonlinear systems

In general, the NOFRFs of nonlinear systems can be evaluated using the GALEs as follows:

Step 1: Determine the GALEs of a NARX or NDE model of the nonlinear system under study using Proposition 1 or Proposition 2.

Step 2: Solve the GALEs (14) or (24) recursively to find the system n th order nonlinear output $y_n(k)$ or $y_n(t)$.

Step 3: Evaluate the n th order NOFRF by computing the ratio of $Y_n(\mathrm{j}\omega)$ and $U_n(\mathrm{j}\omega)$ as defined by (6).

For example, consider the discretised unplugged Van der Pol system (17) under the sampling frequency of $f_s = 1/\Delta t = 512$ Hz subject to the band limited input

$$u(k) = \frac{0.3}{\pi} \frac{\sin\left[200(k\Delta t - 3)\right] - \sin\left[50(k\Delta t - 3)\right]}{k\Delta t - 3} \tag{26}$$

with $k\Delta t \in [0, 6]$ s, the NOFRFs of system (17) can be evaluated using the GALEs based approach as below.

In Step 1, according to Proposition 1, the GALEs of system (17) associated with the system nonlinear outputs up to the 5th order are obtained as

$$\begin{cases} y_1(k) = c_{0,1}(1)u(k-1) + c_{1,0}(1)y_1(k-1) + c_{1,0}(2)y_1(k-2) \\ y_3(k) = c_{1,0}(1)y_3(k-1) + c_{1,0}(2)y_3(k-2) + c_{3,0}(1,1,1)y_1^3(k-1) \\ \quad + c_{3,0}(1,1,2)y_1(k-2)y_1^2(k-1) \\ y_5(k) = c_{1,0}(1)y_5(k-1) + c_{1,0}(2)y_5(k-2) + 2c_{3,0}(1,1,1)y_1^2(k-1)y_3(k-1) \\ \quad + 2c_{3,0}(1,1,2)y_1(k-1)y_1(k-2)y_3(k-1) + c_{3,0}(1,1,1)y_3(k-1)y_1^2(t-1) \\ \quad + c_{3,0}(1,1,2)y_3(k-2)y_1^2(t-1) \end{cases} \tag{27}$$

In Step 2, the GALEs (27) are solved recursively to determine $y_n(k)$ for $n = 1,3,5$. Then the nDTFT of the results is evaluated to get $Y_n(\mathrm{j}\omega)$, $n = 1,3,5$.

With the values of the parameters in the discretized Van der Pol system (17) given as $m = 1$ kg, $c = 30$ Ns/m, $k = 1\times10^4$ N/m and $c_E = 1\times10^7$ Ns/m^3, the sum of the spectra of the solutions to the GALEs (27) when taking into account the system 1st order output $y_1(k)$ (N=1), the 1st and 3rd order outputs $y_1(k)$ and $y_3(k)$ (N=3), and the 1st, 3rd, and 5th order outputs $y_1(k)$, $y_3(k)$ and $y_5(k)$ (N=5), respectively, is evaluated and shown in Fig.2. The results indicate that the sum of spectra of the solutions to the GALEs up to an appropriate order N can well represent the system output spectrum thus verify the effectiveness of the new GALEs concept and its evaluation method given by Proposition 1.

In Step 3, the NOFRFs of system (17) are determined as

$$G_n(\mathrm{j}\omega) = \frac{Y_n(\mathrm{j}\omega)}{U_n(\mathrm{j}\omega)}, n = 1,3,5 \tag{28}$$

using $Y_n(\mathrm{j}\omega)$ obtained in Step 2 and $U_n(\mathrm{j}\omega)$, the nDTFT of $u^n(k)$, for $n = 1,3,5$, with $u(k)$ given in (26).

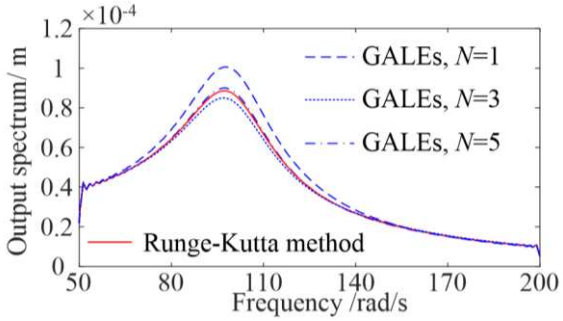

Fig.2 The accurate output spectrum of system (17) and the result evaluated by a sum of solutions to GALEs up to order N

The first three orders' NOFRFs, $G_1(\mathrm{j}\omega), G_3(\mathrm{j}\omega)$ and $G_5(\mathrm{j}\omega)$ of system (17) under input (26) are evaluated by the traditional LS based method [15] and shown in Fig.3. These results are compared with the results evaluated using the GALEs. In the LS evaluation, three inputs of $u_i(k)=\alpha_i u(k), i=1,2,3$ with different amplitude formulated by $\alpha_i=\{0.8,1,1.2\}$ are applied.

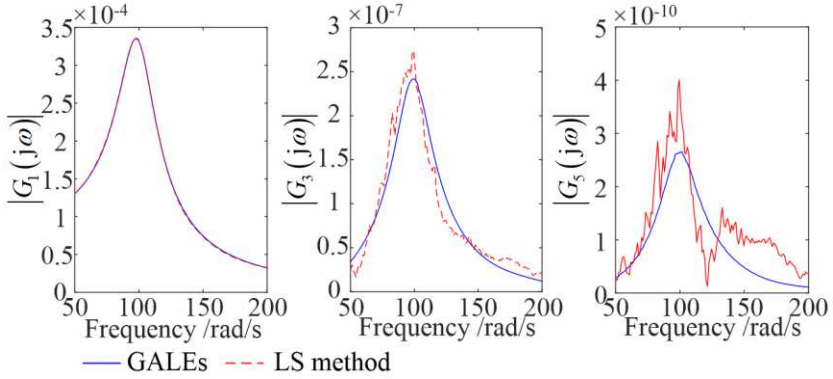

Fig.3 The LS and GALEs based evaluation of the NOFRFs of system (27)

The results in Fig.3 indicate that the traditional LS based evaluation can accurately determine lower order NOFRFs but may induce significant errors when evaluating higher order NOFRFs while the GALEs based method can accurately evaluate the NOFRFs up to an arbitrarily high order of interest.

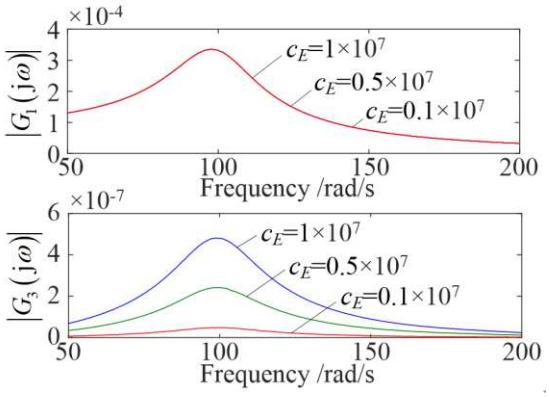

Fig.4 The NOFRFs of system (17) under different values of the system nonlinear damping parameter c_E

In addition, Fig.4 shows the evaluated first and third order NOFRFs of the discretised Van der Pol system (17) with the system nonlinear damping parameter c_E varying over three different values of $c_E=\{0.1,0.5,1\}\times10^7$ Ns/m^3. The results show that:

(i) The NOFRFs provide a series of Bode Plot like diagrams to represent the frequency domain characteristics of nonlinear systems,

(ii) The third order NOFRF can be used to represent the variations in the system nonlinear damping parameter c_E.

These observations of Fig.4 imply that the GALEs based NOFRFs evaluation can significantly facilitate the application of the NOFRFs to the condition monitoring and fault diagnosis of engineering systems and structures. The basic idea is:

- To establish a data driven NARX model of the system under study using a nonlinear system identification method.
- To apply Proposition 1 to the established NARX model and evaluate the NOFRFs of the system, and
- To compare the NOFRFs or an associated index with a base line to monitor the changes in the system characteristics for the purpose of condition monitoring and fault diagnosis.

It is worth noting that although the NARX model parameters can sometimes also be used to monitor the underlying system, the identified NARX model may not be unique while the system frequency domain representation including the NOFRFs is a unique representation of the system dynamics [25]. This implies that the evaluation of the NARX model's NOFRFs index can be a more effective approach that can be used to monitor the conditions of the underlying system [16].

In the following section, two experimental studies will be carried out to demonstrate how to apply the new GALEs based NOFRFs evaluation in conjunction with a nonlinear system identification procedure [25] to monitor the fatigue damage of train wheels and cutting tool wearing conditions in a manufacturing system, respectively.

4. Condition monitoring of railway and manufacturing systems

4.1 Application to the monitoring of fatigue damage of train wheels

The quality of train wheels is significant to the safety of high speed trains [31,32]. With the increase of the working time of train wheels, fatigue damage will accumulate and grow. Specifically, after long-time and high load working, significant fatigue damage will appear. Then micro-cracks will form and expand into macro cracks, which may cause serious accidents [33]. It is therefore important to conduct non-destructive testing on train wheels to regularly monitor the fatigue damage condition.

In this experimental study, 7 train wheels with different working times (starting to be used continuously from year 2005, 2006, 2007, 2008, 2009, 2012 and 2013, respectively) were investigated. Impulse tests were conducted on the wheels as illustrated in Fig.5, so that the wheels' dynamic characteristics over a wide frequency band were excited.

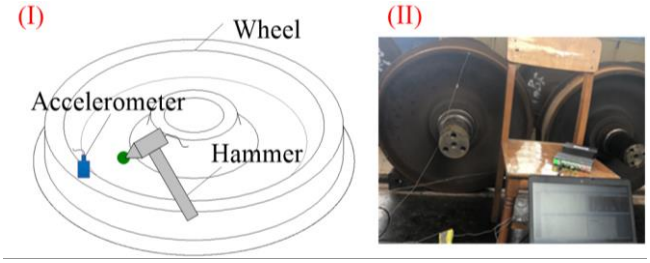

Fig.5 The train wheel and the test samples in the experiment

(I): An illustration of the test; (II): The testing process

In the tests, the impulse excitation was generated by a hammer, and the acceleration response was measured by an accelerometer fitted on the wheel. 10 repeated tests were conducted on each of the 7 train wheels, and the input and output data from each test were collected. For example, one set of input and output data is as shown in Fig.6.

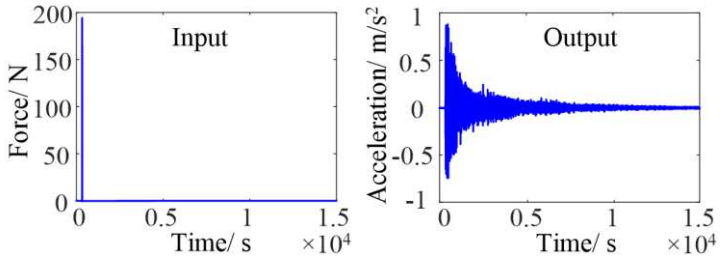

Fig.6 The impulse excitation and acceleration response from a testing on the train wheel starting to be used in 2008

The application study involves three steps.

First, a NARX model under sampling frequency of $f_s = 16384$ Hz was identified using the input and output data collected from each test and the NARMAX identification method for nonlinear system identification [25].

Then the first three orders NOFRFs were computed for each identified model using newly proposed GALEs based approach and

$$u(k) = \frac{0.1}{\pi} \frac{\sin\left(4\times10^4\left(k\Delta t - 1\right)\right) - \sin\left(100\left(k\Delta t - 1\right)\right)}{k\Delta t - 1} \tag{29}$$

with $k\Delta t \in [0, 2]$ s, which covers all dominant frequencies of $\omega \in \left[100, 4\times10^4\right]$ rad/s with the train wheels. The first three orders NOFRFs of the NARX model of the wheel starting to be used in year 2006 are shown in Fig.7.

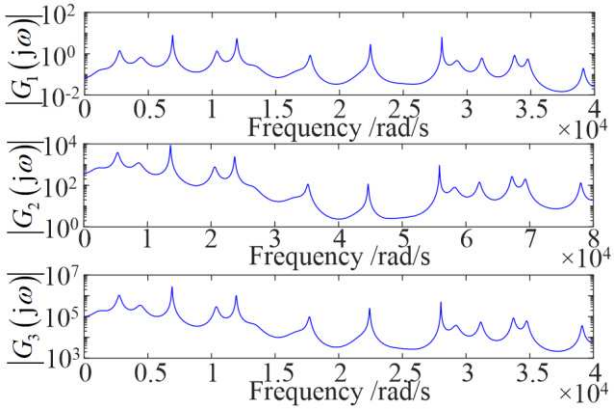

Fig.7 The first three orders NOFRFs of the NARX model of the wheel starting to be used in year 2006

After that, the NOFRFs based indices to the fatigue damage of train wheels [18]

$$Fe_n = \frac{\int_0^{\pi f_s} \left|G_n(\mathrm{j}\omega)\right| \mathrm{d}\omega}{\sum_{i=1}^{3} \int_0^{\pi f_s} \left|G_i(\mathrm{j}\omega)\right| \mathrm{d}\omega}, n = 1,2,3 \tag{30}$$

were used to quantitatively assess the extent to which the fatigue damage has been accumulated.

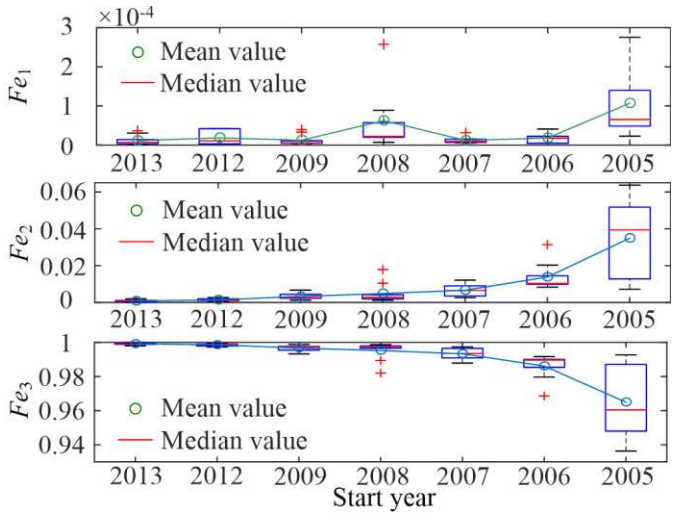

Fig.8 The values of the fatigue damage indices Fe_n

For each train wheel that has been tested, the mean, median, and standard deviation of the indices (30) evaluated using data collected from the 10 repeated tests on the wheel were obtained. The results are shown in Fig.8 against the year when the wheel started to be used.

It can be seen from Fig.8 that, the 2nd and 3rd order NOFRFs related indices both monotonically increase/ decrease with the time scale over which the train wheels were literally used in practice. Considering that fatigue damage normally increases with operational time, the results in Fig.8 demonstrate that the NOFRFs indices evaluated using the new GALEs based approach can be effectively used to monitor fatigue damage conditions of train wheels and, therefore, have good potential to be applied in railway industry.

Moreover, the results in Fig.8 also show that the second and the third order NOFRFs based indices have high sensitivities to the fatigue damage of train wheels, for example, the mean value of the second order index increases 36.92% from the year 2008 to 2007, and 152.64% from the year 2006 to 2005.

It is worth noting that in practice, a healthy structure is not necessarily a linear system. For example, the healthy and damaged train wheels all have significant third order nonlinearities, while it is the increase of the second order NOFRFs' index in Fig.8 that indicates the possible existence of crack type damage in the wheels.

In order to demonstrate the advantage of the NOFRFs based fatigue damage condition monitoring over traditional approaches, the average power of the traditional FRF over the frequency range of input (29) were evaluated as

$$\int_{100}^{4\times10^4} \left|Y(\mathrm{j}\omega)/U(\mathrm{j}\omega)\right|^2 \mathrm{d}\omega \Big/ \left(4\times10^4 - 100\right)$$

from the test data on the wheels starting to be used in 2005 to 2013, respectively. The results are shown in Fig.9 (a), which clearly indicate that the average power does not increase/decrease monotonically with the time of usage of the train wheels so are not appropriate to be used for fatigue damage monitoring.

Resonant frequencies have also been reported to be sensitive to structure crack type damage [34]. However, in the condition monitoring of train wheels, this simple metric seems not effective. The experimental results indicate that train wheels have multiple resonances so it is not straight forward to find an appropriate resonant frequency for condition monitoring purpose. In this case study, after some investigations, the resonant frequency around 7000 rad/s

is used as an index for the purpose of a comparative study. The results are shown in Fig.9 (b) indicating that this resonant frequency-based index does not change monotonically with the increase of damage severity and is, therefore, less sensitive to the train wheel damage of concern than the NOFRFs based index.

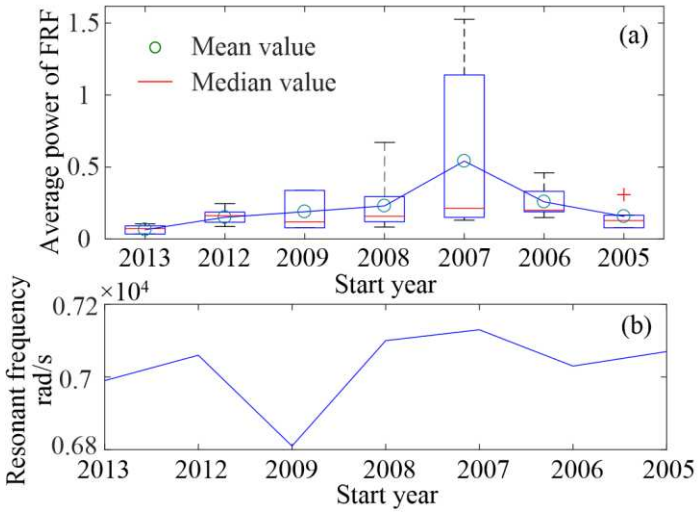

Fig.9 The average power of FRF and a resonant frequency against the time scale of use

In general, the fatigue damage grows with increasing serving time of train wheels, and becomes faulty when damage reaches a certain level. In this study, assume the damage of wheels starting to be used during 2005 to 2007 have been accumulated up to the faulty level when testing was carried out; while wheels starting to be used during 2008 to 2013 are still healthy at the points of testing. The Receiver Operating Characteristic (ROC) curve evaluated using the index Fe_2 is shown in Fig.10, where the healthy condition is labelled as positive. The Area Under Curve (AUC) of the ROC curve is obtained as $AUC = 0.949$, indicating a good performance of the NOFRF index Fe_2 in detection of fault in train wheels. The ROC curve evaluated using the power of FRF as fault detection index is also provided in Fig.10 for a comparison showing a much worse performance than the Fe_2 index.

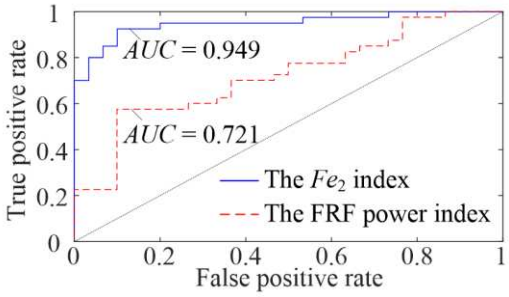

Fig.10 The ROC curves of the NOFRFs and FRF based detection of fault in wheels

4.2 Application to the monitoring of worn cutting tools in a manufacturing system

Worn cutting tools can significantly degrade the surface quality during a milling process [35,36]. As the severity of the wear of cutting tool increases as the working time increases, it is important to monitor wearing conditions so as to detect incipient defects of cutting tools in an early stage.

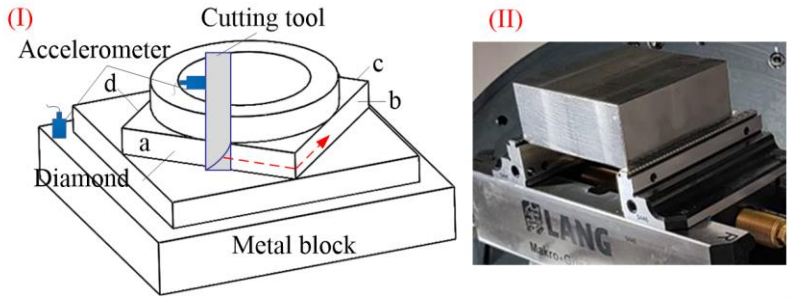

Fig.11 The milling process and test rig in the experiment

(I): Illustration of the milling process and data collection; (II): Metal block to be milled.

In this experimental study, the investigated milling process and the test rig used for monitoring the wear of cutting tools are shown in Fig.11 [37]. Vibration data were collected from two accelerometers fitted on a metal block under the part to be milled and the spindle holding the cutting tool, respectively. The milling is to produce a diamond shaped part as illustrated in Fig.11 (I) from a rectangular metal block shown in Fig.11 (II). a, b, c, d in Fig.11 represent four edges to cut for the diamond part.

The milling experiments were conducted using four different cutting tools which are Health Tool 1 (HT1), Health Tool 2 (HT2), Mild Worn Tool (MWT) and Severe Worn Tool (SWT), respectively, in order to demonstrate how an NOFRFs based condition monitoring can be applied to reveal different cutting tool wearing conditions over different operating time. For each milling process, the vibration data were collected under sampling frequency of $f_s = 102400$ Hz from the two accelerometers. For example, the vibration data collected when HT1 was used are shown in Fig.12, showing that there are R_1 to R_5 five cycles with each cycle having a, b, c, d four stages covering the processes of cutting four different edges of the diamond part.

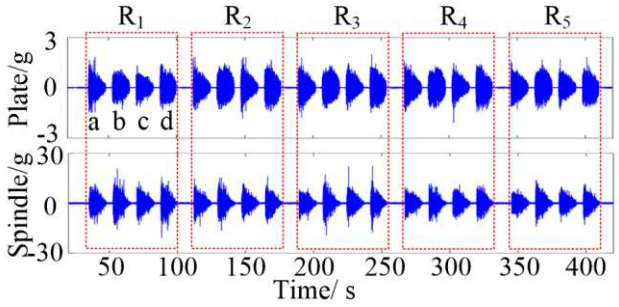

Fig.12 An example of vibration data collected from a milling process

Denote the vibration data collected from the accelerometers fitted on the metal block and spindle as $y_{\text{plate}}(k)$ and $y_{\text{spindle}}(k)$, respectively. Physically, $y_{\text{plate}}(k)$ and $y_{\text{spindle}}(k)$ are two different vibration responses to the electrical power input to the milling process. Therefore, denote the electrical power input as $u(k)$. Then

$$y_{\text{plate}}(k) = N_1[u(k)] \text{ and } y_{\text{Spindle}}(k) = N_2[u(k)] \tag{31}$$

where $N_1[.]$ and $N_2[.]$ represent the dynamic relationship between $y_{\text{plate}}(k)$ and $u(k)$ and between $y_{\text{spindle}}(k)$ and $u(k)$, respectively. Under the condition that a unique inverse operation exists for $N_1[.]$ and $N_2[.]$, it is known that

$$u(k)=N_1^{-1}\left[y_{\text{plate}}(k)\right] \text{ and } u(k)=N_2^{-1}\left[y_{\text{Spindle}}(k)\right] \tag{32}$$

Consequently,

$$\begin{aligned} N_1^{-1}\left[y_{\text{plate}}(k)\right]&=N_2^{-1}\left[y_{\text{Spindle}}(k)\right] \\ y_{\text{plate}}(k)&=N_1\left\{N_2^{-1}\left[y_{\text{Spindle}}(k)\right]\right\}=N\left[y_{\text{Spindle}}(k)\right] \end{aligned} \tag{33}$$

indicating that a dynamic model $N[.]$ can be built to represent the relationship between $y_{\text{plate}}(k)$ and $y_{\text{spindle}}(k)$. Based on these observations, this application study involves the following steps.

First, $y_{\text{plate}}(k)$ and $y_{\text{spindle}}(k)$ were filtered by a band pass filter of $f\in(0,100)$ Hz, and used to build a NARX model using the NARMAX method [25] to represent a dynamic relationship between $y_{\text{plate}}(k)$ and $y_{\text{spindle}}(k)$. For each of the four milling processes associated with the use of HT1, HT2, MWT and SWT, respectively, 20 NARX models were identified. Each NARX model was determined from the data collected from one of the 20 milling stages $\mathrm{R}_i(\mathrm{a}),\ldots,\mathrm{R}_i(\mathrm{d})$, $i=1,\ldots,5$ as shown in Fig.12.

Secondly, the first and second order NOFRFs of the identified NARX models of the milling system were evaluated by the new GALEs based NARX evaluation under the harmonic input of $y_{\text{spindle}}(k)=\cos(\omega_e k\Delta t)$. Here, at frequency of $\omega_e=70\pi$ rad/s is the first dominant frequency of the milling system.

After that, the statistics of mean, median, and standard deviation of the evaluated NOFRFs from the 20 identified NARX models were computed for each of the four milling processes associated with the use of HT1, HT2, MWT and SWT, respectively. The results are shown in Fig.13.

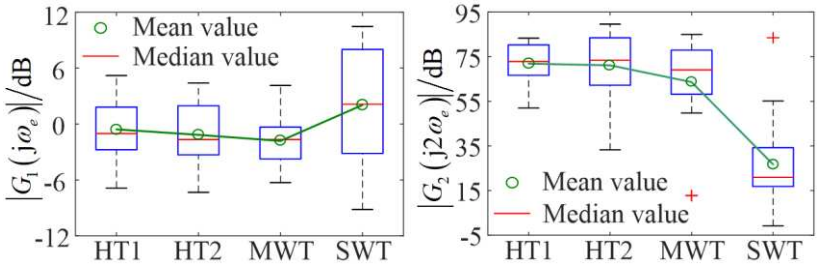

Fig.13 The box plot of the first and the second order NOFRFs

It can be seen from Fig.13 that, the median and mean values of the second order NOFRFs are about the same for health cutting tools but these statistics monotonously decrease against the severity of the wear of cutting tools, demonstrating that the proposed NOFRFs based analysis can be applied to effectively monitor the wearing conditions of cutting tools.

Again for a comparison of the NOFRFs based analysis with using traditional signal analysis, the statistics of mean, median, and standard deviation of the Root Mean Square (RMS) values of the spindle acceleration data over the 20 milling stages of $\mathrm{R}_i(\mathrm{a}),\ldots,\mathrm{R}_i(\mathrm{d})$, $i=1,\ldots,5$ were evaluated for the milling process associated with HT1, HT2, MWT and SWT, respectively. The results are shown in Fig.14 indicating that the RMS value does not increase/decrease monotonically with the increase of severity of wear so cannot be used to monitor the wearing conditions of cutting tools.

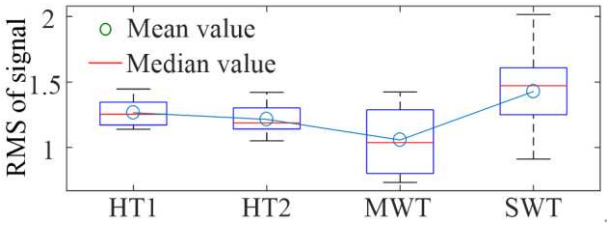

Fig.14 Box plot of the RMS values of spindle acceleration data against the increase of severity of wear of cutting tools

Moreover, the sensitivities of the results in Fig. 10 are evaluated showing that the second order NOFRF value decreases 10.57% from HT2 to MWT, while 58.03% from MWT to SWT.

The classification of the healthy cutting tools (HT1, HT2) and the worn cutting tools (MWT, SWT) using $\left|G_2\left(\mathrm{j}2\omega_e\right)\right|$ is evaluated using the ROC curve shown in Fig.15, where healthy cutting tools are labelled as positive, indicating $AUC = 0.789$. The ROC curve with using the RMS of the vibration signal as the fault detection index is also shown in Fig.15, indicating RMS cannot be used in this case for fault detection.

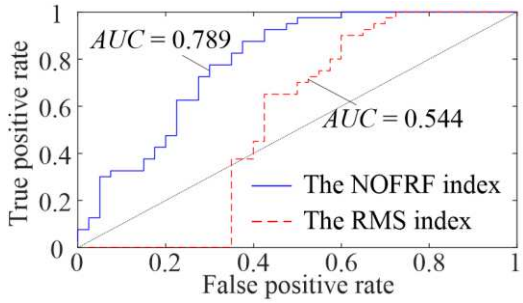

Fig.15 The ROC curves of the NOFRFs and RMS based detection of fault in cutting tools

6. Conclusions

The FRF is a well-known concept in system science and control engineering and has been widely applied in linear system analysis and design. The direct extension of the FRF to nonlinear systems is the GFRFs, which are a series of multidimensional functions of frequencies and are, therefore, difficult to be used in engineering practice. In order to resolve this difficulty, many new extensions of the FRF to the nonlinear case have been proposed. One of these is the NOFRFs. The NOFRFs are a series of one dimensional functions of frequency and have already found many practical applications especially in engineering system condition monitoring and fault diagnosis. However, existing methods that can currently be used for the NOFRFs evaluation either cannot accurately determine the NOFRFs up to any order of nonlinearity of concern or involve complicated procedures that are difficult to be implemented for relatively complicated nonlinear systems. To solve these problems, in the present study, a novel approach for the evaluation of the NOFRFs is proposed based on a new concept known as the GALEs. For a wide class of nonlinear systems which can be represented by a NARX or NDE model, the GALEs enable an accurate evaluation of the NOFRFs to be readily implemented by dealing with the solutions to a series of linear difference or differential equations. This can significantly facilitate the NOFRFs based nonlinear system analyses and the application of the NOFRFs to address various engineering problems. A numerical example has verified the effectiveness of the new GALEs based NOFRFs evaluation. Two experimental studies have demonstrated the significance and potential applications of the new

approach to the condition monitoring of railway and manufacturing systems, respectively. The fundamental difference between the NOFRFs based condition monitoring and other signal analysis or simple structural characteristic parameter-based approaches is that the NOFRFs can often more comprehensively reveal inherent structural system properties, providing a better insight into the changes in system characteristics that are induced by various damage or defects.

Appendix A: Proof of Proposition 1

For the convenience of derivation, denote

$$\underset{\omega_1+\cdots+\omega_n=\omega}{\aleph}[.]=\frac{1}{\sqrt{n}(2\pi)^{n-1}}\int_{\omega_1+\cdots+\omega_n=\omega}[.]\mathrm{d}\sigma_\omega \tag{A1}$$

This implies

$$\overline{DF}\left[\prod_{i=1}^{n}w_i(k)\right]=\underset{\omega_1+\cdots+\omega_n=\omega}{\aleph}\left[\prod_{i=1}^{n}W_i(\mathrm{j}\omega_i)\right] \tag{A2}$$

where $W_i(\mathrm{j}\omega)=\overline{DF}\left[w_i(k)\right]=DF\left[w_i(k)\right]\Delta t$ with $DF[.]$ representing the DTFT of $w_i(k)$ [38].

The nth order GFRFs (4) can be written as

$$\Psi_n=\Psi_{n,u}+\Psi_{n,uy}+\Psi_{n,y} \tag{A3}$$

where $\Psi_{n,u},\Psi_{n,uy}$ and $\Psi_{n,y}$ are as given in (10)-(12).

Multiplying $\prod_{i=1}^{n}U(\mathrm{j}\omega_i)$ on both sides of (A3) and then applying the integration operation $\underset{\omega_1+\cdots+\omega_n=\omega}{\aleph}[.]$ yield

$$\begin{aligned}\underset{\omega_1+\cdots+\omega_n=\omega}{\aleph}\left[\Psi_n\prod_{i=1}^{n}U(\mathrm{j}\omega_i)\right]&=\underset{\omega_1+\cdots+\omega_n=\omega}{\aleph}\left[\Psi_{n,u}\prod_{i=1}^{n}U(\mathrm{j}\omega_i)\right]\\&+\underset{\omega_1+\cdots+\omega_n=\omega}{\aleph}\left[\Psi_{n,uy}\prod_{i=1}^{n}U(\mathrm{j}\omega_i)\right]+\underset{\omega_1+\cdots+\omega_n=\omega}{\aleph}\left[\Psi_{n,y}\prod_{i=1}^{n}U(\mathrm{j}\omega_i)\right]\end{aligned} \tag{A4}$$

The left hand side of (A4) can be arranged as

$$\underset{\omega_1+\cdots+\omega_n=\omega}{\aleph}\left[\Psi_n\prod_{i=1}^{n}U(\mathrm{j}\omega_i)\right]=\overline{DF}\left[y_n(k)\right]-\sum_{k_1=1}^{K}c_{1,0}(k_1)\overline{DF}\left[y_n(k-k_1)\right] \tag{A5}$$

The three terms on the right hand side of (A4) are separately discussed as follows.

(A) Hyperplane integration of $\Psi_{n,u}\prod_{i=1}^{n}U(\mathrm{j}\omega_i)$

This term can be written as

$$\begin{aligned}\underset{\omega_1+\cdots+\omega_n=\omega}{\aleph}\left[\Psi_{n,u}\prod_{i=1}^{n}U(\mathrm{j}\omega_i)\right]&=\sum_{k_1,k_n=1}^{K}c_{0,n}(k_1,\cdots,k_n)\underset{\omega_1+\cdots+\omega_n=\omega}{\aleph}\left[\prod_{i=1}^{n}U(\mathrm{j}\omega_i)\exp(-\mathrm{j}k_i\omega_i\Delta t)\right]\\&=\sum_{k_1,k_n=1}^{K}c_{0,n}(k_1,\cdots,k_n)\overline{DF}\left[\prod_{i=1}^{n}u(k-k_i)\right]\end{aligned} \tag{A6}$$

(B) Hyperplane integration of $\Psi_{n,y}\prod_{i=1}^{n}U\left(\mathrm{j}\omega_i\right)$

Denote

$$\underset{\omega_1+\cdots+\omega_n=\omega}{\aleph}\left[H_{n,p}^{\mathbf{K}_p}\left(\omega_1,\cdots,\omega_n\right)\prod_{i=1}^{n}U\left(\mathrm{j}\omega_i\right)\right]=\overline{DF}\left[y_{n,p}^{\mathbf{K}_p}\left(k\right)\right] \tag{A7}$$

where $p=2,\ldots,n$, and according to (4) and (5),

$$\overline{DF}\left[y_{n,1}^{\mathbf{K}_1}\left(k\right)\right]=\underset{\omega_1+\cdots+\omega_n=\omega}{\aleph}\left[H_{n,1}^{\mathbf{K}_1}\left(\omega_1,\cdots,\omega_n\right)\prod_{i=1}^{n}U\left(\mathrm{j}\omega_i\right)\right]=\overline{DF}\left[y_n\left(k-k_1\right)\right] \tag{A8}$$

Therefore, using (12) and (A7), the third term on the right hand side of (A4) can be arranged as

$$\underset{\omega_1+\cdots+\omega_n=\omega}{\aleph}\left[\Psi_{n,y}\prod_{i=1}^{n}U\left(\mathrm{j}\omega_i\right)\right]=\sum_{p=2}^{n}\sum_{k_1,\,k_p=1}^{K}c_{p,0}\left(k_1,\cdots,k_p\right)\overline{DF}\left[y_{n,p}^{\mathbf{K}_p}\left(k\right)\right] \tag{A9}$$

Substituting $H_{n,p}^{\mathbf{K}_p}\left(\omega_1,\cdots,\omega_n\right)$ in (5) into (A7) yields

$$\begin{aligned}\overline{DF}\left[y_{n,p}^{\mathbf{K}_p}\left(k\right)\right]&=\underset{\omega_1+\cdots+\omega_n=\omega}{\aleph}\left[H_{n,p}^{\mathbf{K}_p}\left(\omega_1,\cdots,\omega_n\right)\prod_{i=1}^{n}U\left(\mathrm{j}\omega_i\right)\right]\\&=\sum_{i=1}^{n-(p-1)}\underset{\omega_1+\cdots+\omega_n=\omega}{\aleph}\left\{\left[H_i\left(\omega_1,\cdots,\omega_i\right)\exp\left(-\mathrm{j}k_p\bar{\omega}\Delta t\right)\prod_{j=1}^{i}U\left(\mathrm{j}\omega_j\right)\right]\left[H_{n-i,p-1}^{\mathbf{K}_p}\left(\omega_{i+1},\cdots,\omega_n\right)\prod_{j=i+1}^{n}U\left(\mathrm{j}\omega_j\right)\right]\right\}\\&=\sum_{i=1}^{n-(p-1)}\overline{DF}\left[y_i\left(k-k_p\right)\times y_{n-i,p-1}^{\mathbf{K}_p}\left(k\right)\right]\end{aligned} \tag{A10}$$

with $\omega_1+\cdots+\omega_i=\bar{\omega}$ and $\omega_{i+1}+\cdots+\omega_n=\omega-\bar{\omega}$.

(C) Hyperplane integration of $\Psi_{n,uy}\prod_{i=1}^{n}U\left(\mathrm{j}\omega_i\right)$

The term can be arranged using (11) as

$$\begin{aligned}\underset{\omega_1+\cdots+\omega_n=\omega}{\aleph}\left[\Psi_{n,uy}\prod_{i=1}^{n}U\left(\mathrm{j}\omega_i\right)\right]&=\sum_{q=1}^{n-1}\sum_{p=1}^{n-q}\sum_{k_1,\,k_{p+q}=1}^{K}c_{p,q}\left(k_1,\cdots,k_{p+q}\right)\\&\times\underset{\omega_1+\cdots+\omega_n=\omega}{\aleph}\left[H_{n-q,p}^{\mathbf{K}_{p+q}}\left(\omega_1,\cdots,\omega_{n-q}\right)\prod_{i=1}^{n-q}U\left(\mathrm{j}\omega_i\right)\prod_{i=p+1}^{p+q}U\left(\mathrm{j}\omega_{n-q+i-p}\right)\exp\left(-\mathrm{j}k_i\omega_{n-q+i-p}\Delta t\right)\right]\\&=\sum_{q=1}^{n-1}\sum_{p=1}^{n-q}\sum_{k_1,\,k_{p+q}=1}^{K}c_{p,q}\left(k_1,\cdots,k_{p+q}\right)\overline{DF}\left[y_{n-q,p}^{\mathbf{K}_{p+q}}\left(k\right)\prod_{i=p+1}^{p+q}u\left(k-k_i\right)\right]\end{aligned} \tag{A11}$$

Consequently, by substituting (A5), (A6), (A9) and (A10), as well as (A11) into (A4) and taking the inverse nDTFT on both sides of the equation, the GALEs (14) is reached. Moreover, equation (15a) and (15b) can be obtained from the taking inverse nDTFT of (A10) and (A8), respectively. Thus, Proposition 1 is proven.

Acknowledgement

This work was supported by the UK EPSRC and Royal Society.

References

[1] P. J. Antsaklis, A. N. Michel, Linear systems, Springer Science & Business Media, 2006.

[2] S. Thenozhi, Y. Tang, Nonlinear frequency response based adaptive vibration controller design for a class of nonlinear systems. Mech. Syst. Signal Proc. 99 (2018) 930-945. https://doi.org/10.1016/j.ymssp.2017.03.017

[3] D. A. George, Continuous nonlinear systems (No. TR-355). Massachusetts Inst of Tech Cambridge Research Lab of Electronics, 1959.

[4] K. Worden, Nonlinearity in structural dynamics: detection, identification and modelling, CRC Press, 2019.

[5] B. Xiao, C. Gao, Z. G. Liu, Decoupling analysis on nonlinear system based on the modified generalized frequency response functions. Mech. Syst. Signal Proc. 42 (2014) 283-299. https://doi.org/10.1016/j.ymssp.2013.05.015

[6] R. van der Weijst, B. van Loon, M. Heertjes, M. Heemels, Scheduled controller design for systems with varying sensor configurations: A frequency-domain approach, IEEE Trans. Control Syst. Technol. 26 (2017) 523-534. https://doi.org/10.1109/TCST.2017.2675838

[7] F. He, S. A. Billings, H. L. Wei, P. G. Sarrigiannis, Y. Zhao, Spectral analysis for nonstationary and nonlinear systems: A discrete-time-model-based approach, IEEE Trans. Biomed. Eng. 60 (2013) 2233-2241. https://doi.org/10.1109/TBME.2013.2252347

[8] Z. Q. Lang, S. A. Billings, Energy transfer properties of non-linear systems in the frequency domain, Int. J. Control. 78 (2005) 345-362. https://doi.org/10.1080/00207170500095759

[9] Z. Q. Lang, S. A. Billings, R. Yue, J. Li, Output frequency response function of nonlinear Volterra systems, Automatica. 43, (2007) 805-816. https://doi.org/10.1016/j.automatica.2006.11.013

[10] D. Rijlaarsdam, T. Oomen, P. Nuij, J. Schoukens, M. Steinbuch, Uniquely connecting frequency domain representations of given order polynomial Wiener-Hammerstein systems, Automatica. 48 (2012) 2381-2384. https://doi.org/10.1016/j.automatica.2012.06.006

[11] C. Ho, Z. Q. Lang, S. A. Billings, Design of vibration isolators by exploiting the beneficial effects of stiffness and damping nonlinearities, J. Sound Vibr. 333 (2014) 2489-2504. https://doi.org/10.1016/j.jsv.2014.02.011

[12] Y. P. Zhu, Z. Q. Lang, Design of nonlinear systems in the frequency domain: an output frequency response function-based approach, IEEE Trans. Control Syst. Technol. 99 (2017) 1-14. https://doi.org/10.1109/TCST.2017.2716379

[13] D. Rijlaarsdam, P. Nuij, J. Schoukens, M. Steinbuch, A comparative overview of frequency domain methods for nonlinear systems, Mechatronics. 42 (2017)11-24. https://doi.org/10.1016/j.mechatronics.2016.12.008

[14] R. S. Bayma, Y. P. Zhu, Z. Q. Lang, The analysis of nonlinear systems in the frequency domain using Nonlinear Output Frequency Response Functions, Automatica. 94 (2018) 452-457. https://doi.org/10.1016/j.automatica.2018.04.030

[15] Z. K. Peng, Z. Q. Lang, S. A. Billings, Crack detection using nonlinear output frequency response functions, J. Sound Vibr. 301 (2007) 777-788. https://doi.org/10.1016/j.jsv.2006.10.039

[16] Z. K. Peng, Z. Q. Lang, C. Wolters, S. A. Billings, K. Worden, Feasibility study of structural damage detection using NARMAX modelling and Nonlinear Output Frequency Response Function based analysis. Mech. Syst. Signal Proc. 25 (2011) 1045-1061. https://doi.org/10.1016/j.ymssp.2010.09.014

[17] X. Y. Zhao, Z. Q. Lang, G. Park, C. R. Farrar, M. D. Todd, Z. Mao, K. Worden, A new transmissibility analysis method for detection and location of damage via nonlinear features in MDOF structural systems. IEEE-ASME Trans. Mechatron. 20 (2015)1933-1947. https://doi.org/10.1109/TMECH.2014.2359419

[18] H. Mao, W. Tang, Y. Huang, D. Yuan, Z. Huang, X. Li, W. Zheng, S. Ma, The construction and comparison of damage

detection index based on the nonlinear output frequency response function and experimental analysis, J. Sound Vibr. 427 (2018) 82-94. https://doi.org/10.1016/j.jsv.2018.04.028

[19] Y. Liu, Y. L. Zhao, J. T. Li, H. Ma, Q. Yang, X. X. Yan, Application of weighted contribution rate of nonlinear output frequency response functions to rotor rub-impact. Mech. Syst. Signal Proc. 136 (2020) 106518. https://doi.org/10.1016/j.ymssp.2019.106518

[20] S. Zhang, Z. Q. Lang, SCADA-data-based wind turbine fault detection: A dynamic model sensor method, Control. Eng. Practice. 102 (2020) 104546. https://doi.org/10.1016/j.conengprac.2020.104546

[21] W. X. Ren, Z. H. Zong, Output-only modal parameter identification of civil engineering structures, Struct. Eng. Mech. 17 (2004) 429-444. http://dx.doi.org/10.12989/sem.2004.17.3_4.429

[22] B. Sanchez, E. Louarroudi, E. Jorge, J. Cinca, R. Bragos, R. Pintelon, A new measuring and identification approach for time-varying bioimpedance using multisine electrical impedance spectroscopy, Physiol. Meas. 34 (2013) 339. http://dx.doi.org/10.1088/0967-3334/34/3/339

[23] J. V. Feijoo, K. Worden, R. Stanway, System identification using associated linear equations, Mech. Syst. Signal Proc. 18 (2004) 431-455. https://doi.org/10.1016/S0888-3270(03)00078-5

[24] J. V. Feijoo, K. Worden, R. Stanway, Associated linear equations for Volterra operators, Mech. Syst. Signal Proc. 19 (2005) 57-69. https://doi.org/10.1016/j.ymssp.2004.03.003

[25] S. A. Billings, Nonlinear system identification: NARMAX methods in the time, frequency, and spatio-temporal domains. John Wiley & Sons, 2013.

[26] J. C. Peyton-Jones, S. A. Billings, Recursive algorithm for computing the frequency response of a class of non-linear difference equation models, Int. J. Control. 50 (1989) 1925-1940. https://doi.org/10.1080/00207178908953474

[27] Z. Q. Lang, S. A. Billings, Output frequency characteristics of nonlinear systems, Int. J. Control. 64 (1996) 1049-1067. https://doi.org/10.1080/00207179608921674

[28] Y. P. Zhu, Z. Q. Lang, A new convergence analysis for the Volterra series representation of nonlinear systems, Automatica. 111 (202) 108599. https://doi.org/10.1016/j.automatica.2019.108599

[29] B. Tang, M. J. Brennan, A comparison of the effects of nonlinear damping on the free vibration of a single-degree-of-freedom system, J. Vib. Acoust.-Trans. ASME. 134 (2013) 024501. https://doi.org/10.1115/1.4005010

[30] S. A. Billings, J. C. Peyton-Jones, Mapping non-linear integro- differential equations into the frequency domain, Int. J. Control. 52 (1990) 863-879. https://doi.org/10.1080/00207179008953572

[31] D. Zhou, H. Ji, X. He, J. Shang, Fault detection and isolation of the brake cylinder system for electric multiple units, IEEE Trans. Control Syst. Technol. 26 (2017)1744-1757. https://doi.org/10.1109/TCST.2017.2718979

[32] K. Makino, S. Biwa, Influence of axle–wheel interface on ultrasonic testing of fatigue cracks in wheelset, Ultrasonics. 53 (2017) 239-248. https://doi.org/10.1016/j.ultras.2012.06.007

[33] H. Mao, W. Tang, W. Zhu, G. Yang, X. Li, Z. Huang, H. Mao, B. Si, Feasibility study on wheelset fatigue damage with NOFRFs-KL divergence detection method in SIMO. J. Sound Vibr., 483 (2020) 115447. https://doi.org/10.1016/j.jsv.2020.115447

[34] L. G. Villani, S. da Silva, A. Cunha, M. D. Todd, On the detection of a nonlinear damage in an uncertain nonlinear beam using stochastic Volterra series. Struct. Health Monit., 19 (2020), 1137-1150. https://doi.org/10.1177/1475921719876086

[35] N. J. van Dijk, N. van de Wouw, E. J. Doppenberg, H. A. Oosterling, H. Nijmeijer, Robust active chatter control in the high-speed milling process, IEEE Trans. Control Syst. Technol. 20 (2011) 901-917. https://doi.org/10.1109/TCST.2011.2157160

[36] G. Zhang, S. To, S. Zhang, Relationships of tool wear characteristics to cutting mechanics, chip formation, and surface quality in ultra-precision fly cutting, Int. J. Adv. Manuf. Technol. 83 (2016) 133-144. http://dx.doi.org/10.1007%2Fs00170-015-7483-6

[37] Y. P. Zhu, Z. Q. Lang, H. Laalej, Data driven evaluation of nonlinear output frequency response functions with applications to structural system fault diagnosis. In 2019 1st International Conference on Industrial Artificial Intelligence (IAI) (pp. 1-6). IEEE.

[38] A. Poularikas, The Transforms and Applications: Handbook. The Electrical Engineering Handbook Series. Taylor & Francis Group, 2000.